

# We are IntechOpen, the world's leading publisher of Open Access books Built by scientists, for scientists

6,900

Open access books available

186,000

International authors and editors

200M

Downloads

Our authors are among the

154

Countries delivered to

TOP 1%

most cited scientists

12.2%

Contributors from top 500 universities



WEB OF SCIENCE™

Selection of our books indexed in the Book Citation Index  
in Web of Science™ Core Collection (BKCI)

Interested in publishing with us?  
Contact [book.department@intechopen.com](mailto:book.department@intechopen.com)

Numbers displayed above are based on latest data collected.  
For more information visit [www.intechopen.com](http://www.intechopen.com)



---

# Study of Green Nanoparticles and Biocomplexes Based on Exopolysaccharide by Modern Fourier Transform Spectroscopy

---

Goran S. Nikolić, Milorad D. Cakić, Slobodan Glišić,  
Dragan J. Cvetković, Žarko J. Mitić and  
Dragana Z. Marković

Additional information is available at the end of the chapter

<http://dx.doi.org/10.5772/64611>

---

## Abstract

The intention of this chapter is to contribute in clarification of nanoparticle synthesis and biocomplexes based on exopolysaccharide, green synthetic method development, their physico-chemical characterization by modern spectroscopy, as well as testing of their antimicrobial activity. Silver nanoparticles of polysaccharide type have scientific interest, but practical importance too, because of their application in pharmaceutical and cosmetic product development due to proven antimicrobial and antioxidant activities. On the other hand, the biocomplexes based on exopolysaccharides are important in treatment of biometal deficiency in human and veterinary medicine, as well as in metal ion transporting in organism. Despite a number of studies of this kind of complexes, the investigations of effect of their structure to pharmaco-biological activity are still interesting. It is important that question of interaction between reducing and stabilizing agents with metal ions is still opened. In this respect, the presented chapter offers further progress in the examination of silver nanoparticles and cobalt biocomplex synthesis with dextran oligosaccharides and its derivatives (such as dextran sulfate and carboxymethyl dextran). The complex structure, spectroscopic characterization, and the spectra-structure correlation have been analyzed by different Fourier transform infrared (FTIR) spectroscopic techniques combined with energy-dispersive X-ray (EDX), X-ray diffraction (XRD), scanning electron microscopy (SEM), and surface plasmon resonance UV-Vis methods.

**Keywords:** nanoparticles, biocomplexes, polysaccharides, silver, cobalt, FTIR spectroscopy

---

## 1. Introduction

Investigation of nanoparticles by different methods, especially by Fourier transform infrared (FTIR) spectroscopy, is very interesting in last years since they have a wide potential application in different industries [1–5]. Thus, silver nanoparticles (AgNP) of polysaccharide type and other natural products have scientific interest, but practical importance too, because of their application in pharmaceutical and cosmetic products development due to proven antimicrobial and antioxidant activities [6–9]. The nanoparticles are commonly synthesized by silver (or other metals) ions reduction to elementary state. But, reducing agents should also possess stabilizing properties in order to prevent aggregation [1]. Bankura and coworkers described a simple method of AgNP synthesis at room temperature from dextran, as well as their characterization and microbiological activity [6]. Pullulan-mediated Ag nanoparticles, their synthesis, characterization, and microbiological activities are also reported [4]. Soluble starch, starch-like polysaccharides, and chitosan are used in AgNP synthesis [5–9]. AgNP chitosan/gelatin bionanocomposites have also been studied [5]. Compounds containing carbonyl group are relatively easy complexed with different metals [10–12]. This functional group contains some polysaccharide derivatives like carboxymethyl cellulose (CMC) or carboxymethyl dextran (CMD), which are obtained by different chemical reactions of proton exchange between OH groups of glucoside moiety and carboxymethyl groups. AgNP-CMC nanoparticles were prepared in weak alkaline solution by reaction of  $\text{AgNO}_3$  with CMC as a reducing and capping agent. It has been established that size distribution and morphology of mentioned nanoparticles are depended on Ag: CMC weight ratio, reaction time, temperature, and pH value of the reaction system. FTIR spectrophotometric analysis has shown that interactions between AgNP and polysaccharide have steric character [13]. Studies of composite hydrazine-CMD and CMD magnetic Fe-based nanoparticles [14, 15] have shown that solubility of these nanoparticles depends on pH value (NaOH), not on CMD content. This fact indicates on strong interactions of carbonyl group with magnetic nanoparticles on the surface.

Hence, there are indications that carboxymethyl dextran form nanoparticles with Ag ions. CMD possess COOH group which can react with positively charged Ag ions to form complex compounds, but, it can also reduce Ag ions and stabilize the formed nanoparticles as in the case of hyaluronic acid with AgNP [16]. Since CMD has the ability to form nanoparticles, the intention of this chapter is to contribute in clarification of AgNP synthesis, physico-chemical characterization by FTIR spectroscopic, diffraction and chromatographic methods, as well as testing of their antimicrobial activity. On the other hand, the biocomplexes based on exopolysaccharides are important in treatment of biometals deficiency in human and veterinary medicine [1, 17]. Polysaccharides, oligosaccharides and their derivatives, as well as simple sugars, may be used as ligands for the synthesis of biocomplexes with different metal ions (Cu, Fe, and Zn). These biocomplexes have an important role in metal ions transporting in organism [18]. Despite a number of studies of this kind of complexes, the investigations of effect of their structure to pharmaco-biological activity are still interesting [19]. In this respect, the presented chapter offers further progress in the investigation of cobalt complex synthesis with dextran oligosaccharide, spectroscopic characterization, and the spectra-structure correlation by various FTIR techniques.

## 2. Green nanoparticles of silver

Recent investigations of nanoparticles synthesis are mostly directed to green synthetic methods development. These methods include nontoxic reagents, synthesis procedures without problematic side products, and especially usage of biodegradable materials. Thus, chemical reduction in silver ions is the most frequently used besides photochemical or electrochemical methods [1]. In order to reduce and stabilize the Ag nanoparticles, the polysaccharides (dextran, starch, pullulan, cellulose) and their derivatives (dextran sulfate-DS, carboxymethyl cellulose, carboxymethyl dextran, chitosan, hyaluronic acid, heparin), and biocomposites AgNP chitosan/gelatin, are developed and improved [2–6, 13, 14, 16, 20–25]. Characterization of these particles has been carried out by UV-Vis, FTIR spectroscopy, X-ray diffraction (XRD), and energy-dispersive X-ray (EDX) methods. Electronic microscopy techniques [scanning electron microscopy (SEM) and TEM] are used for particle size determination and distribution, as well as shape defining. It is interesting that question of interaction nature between reducing and stabilizing agents with AgNP is still opened. Some authors [13] consider that steric physical interactions are relevant, while others [2, 16] give an explanation via coordination complex of Ag ions with reducing and stabilizing agents which contain suitable functional groups (COOH, NH<sub>2</sub>, OH, OSO<sub>3</sub>H), as in the case of Cu(II) ions complexes with carboxymethyl dextran or dextran sulfate (Figure 1).

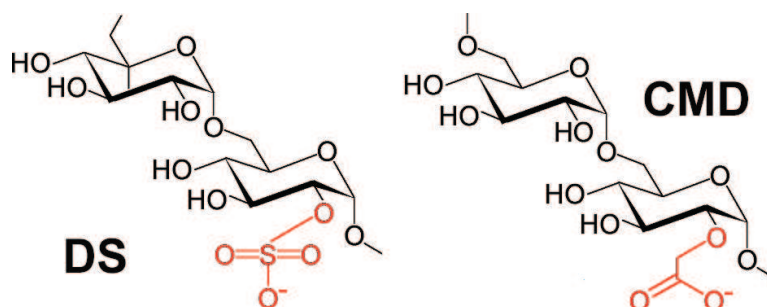


Figure 1. Structural fragment of dextran sulfate sodium salt (DS) and carboxymethyl dextran (CMD) molecule.

Having in mind these facts, it can be assumed that dextran sulfate, which contains one or more sulfo groups in its structure, can be used as reducing and stabilizing agent for the AgNP synthesis. Also, it may be assumed that dextran sulfate forms complexes similar to CMD about what there are no literature data. Therefore, investigations in this chapter are related to the AgNP-DS and AgNP-CMD synthesis, their characterization by different methods and antimicrobial activity determination.

### 2.1. Synthesis procedure

The synthesis of AgNP-DS has been performed in a reactor at temperature of 100°C, during 240 min, at constant pH of 7.5 and continuously stirring. Dextran sulfate has been used as a ligand in the synthesis. The synthesis is performed by DS solution (100 cm<sup>3</sup>, 0.002 M)

adding in 100 cm<sup>3</sup> of AgNO<sub>3</sub> solution (0.001 M). The complex formation has been monitored via changing of reaction solution color, from white to yellow. The AgNP-DS complex was precipitated with 96% ethanol after cooling down the reaction mixture to the room temperature. The obtained product has been dried at 105°C under vacuum during 180 min. On the other hand, the carboxymethyl dextran has been used in the case of the AgNP-CMD complex synthesis. The synthesis has been performed by 100 cm<sup>3</sup> of AgNO<sub>3</sub> (0.001 M) solution adding in 200 cm<sup>3</sup> of CMD ligand solution (0.002 M) at constant pH of 7.0 (adjusted by NaOH). The synthesis is performed to the defined M:L ratio (from 1:1 to 1:2) by changing of reagents volume. The complexation has been performed at 100°C and continuously stirring during 120 min. A successful outcome of the AgNP-CMD complex synthesis has been identified by changing of reaction solution color, from white to yellow. The reaction mixture has kept under reflux 24 h more, after that it has cooled to room temperature, and the complex AgNP-CMD has precipitated by 96% ethanol. Final product has been dried at 105°C under vacuum during 180 min. The prepared AgNP-DS and AgNP-CMD complexes were characterized by different methods (FTIR, UV-Vis, SEM, XRD, EDX) and by antimicrobial activity.

## 2.2. FTIR study

The FTIR spectra were recorded by BOMEM MB-100 (Hartmann & Braun, Canada) FTIR spectroscope and by KBr technique, at room temperature with 2 cm<sup>-1</sup> resolution. Spectra-structure correlation has been performed on empirical manner [2, 22], by comparing the spectra of ligands (DS and CMD) with the spectra of their complexes (AgNP-DS and AgNP-CMD). The appropriate FTIR spectra are shown in **Figures 2** and **3**.

The results of the complex AgNP-DS spectral analysis are shown in **Table 1**. They show the position and assignments of bands that come from vibrations of all types of sulfo groups in DS and AgPN-DS, as well as bands of deformation CH vibrations outside of the plane of glucopyranose unit which are characteristic for its conformation determining. As it can be seen in **Table 1**, there is a difference in the position of the  $\nu_{as}(S-O)$  band which is shifted ~22 cm<sup>-1</sup> toward lower frequencies in the AgPN-DS spectrum (**Figure 2**), as well as the band from  $\nu_{as}(O-S-O)$  which is shifted ~8 cm<sup>-1</sup> toward higher frequencies. This difference in the bands position indicates the formation of coordination complexes between Ag ions and DS, where there is a change in conformation of sulfo groups from Eq to Ax position. The appearance of the spectrum in the area of C-CH out-of-plane deformational vibrations surface coupled with C-C-O, O-C-O and C-O-C vibrations depends on glucopyranose unit conformation [25–27]. When it is <sup>4</sup>C<sub>1</sub> conformation, the bands at ~915 cm<sup>-1</sup> (weak), 850 cm<sup>-1</sup> (shoulder), and 752 cm<sup>-1</sup> are expected in the spectrum. The results from **Table 1** show that starting DS retains the same conformation of glucopyranose unit during complex with Ag ions formation. There is a sharp intensive band at 1384 cm<sup>-1</sup> in the FTIR spectrum of AgNP-DS (**Figure 2**) observed by other authors who have investigated similar complexes and given the explanation of its origin [4, 5, 13, 22]. So, in the case of AgNP-CMD complex (**Figure 3c**), some authors consider that this band is a result of  $\nu_s(O-N-O)$  at O=NO<sub>2</sub><sup>-</sup> radicals which are formed from AgNO<sub>3</sub> agents participating in the formation of nanoparticles through the surface interactions [13].

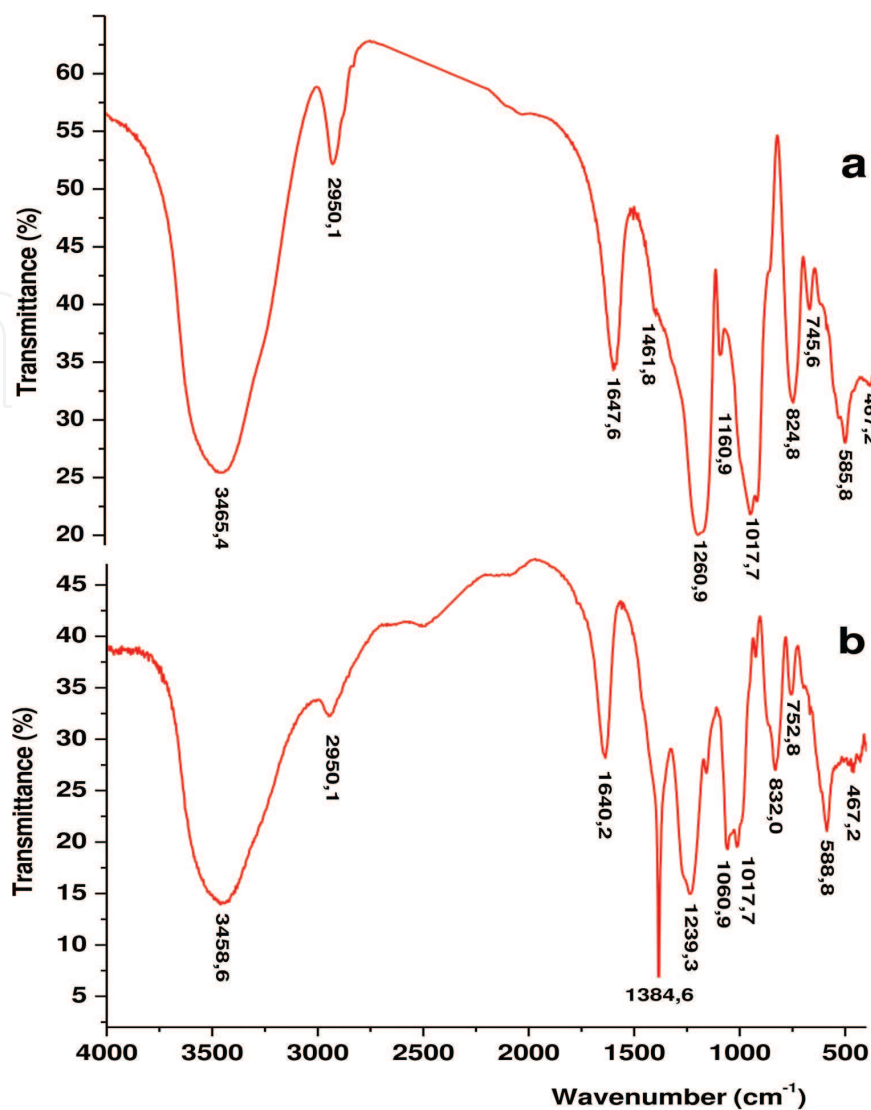


Figure 2. FTIR spectra of dextran sulfate sodium salt (a) and AgNP-DS complex (b).

The infrared spectra of AgNP-CMD products and starting CMD agent are compared with literature data and dextran spectrum because of the major bands assignment (Figure 3). In the CMD spectrum, vibrations of carboxymethyl groups:  $\nu(\text{C}-\text{O})$  around  $1740\text{ cm}^{-1}$ ; deformation vibration  $\delta(\text{C}-\text{OH})$  which appears around  $1250\text{ cm}^{-1}$ ;  $\nu(\text{C}-\text{O})$  vibration around  $1150\text{ cm}^{-1}$ ; and deformation  $\delta(\text{C}-\text{O})$  vibration around  $680\text{ cm}^{-1}$  are expected to oppose starting dextran for CMD synthesis. Stretching  $\nu(\text{C}-\text{O})$  vibration has been found in similar carboxymethyl polysaccharides; after carboxymethylation of the k-carrageenan,  $\nu(\text{C}-\text{O})$  has found at  $1737\text{ cm}^{-1}$  [28], for carboxymethylated glucan at  $1736\text{ cm}^{-1}$  [29], as well as at  $1750\text{ cm}^{-1}$  in the spectrum of CMD [14]. As it can be seen from Figure 3b, the CMD spectra possess bands at  $1740$ ,  $1244$ ,  $1139$ , and  $682\text{ cm}^{-1}$  (which are marked by arrows) from CO carboxymethyl vibration of all types. The aforementioned bands are not in the range of dextran (Figure 3a) as it is expected. Changes in the position of the above-mentioned bands can be a good indicator of bonds type that is eventually formed by interaction with  $\text{Ag}^+$  ions [16]. Also, the changes in the area of deformation vibration of C-OH are expected. In the case of AgNP-CMD coordination com-

plexes formation, the frequency  $\nu(\text{C-O})$  band should be lower, or, if both O atoms of COOH groups participate in the coordination, the frequency of  $\nu(\text{C-O})$  vibration should be higher because of electron delocalization, as well as the absence of  $\delta(\text{C-OH})$  bands.

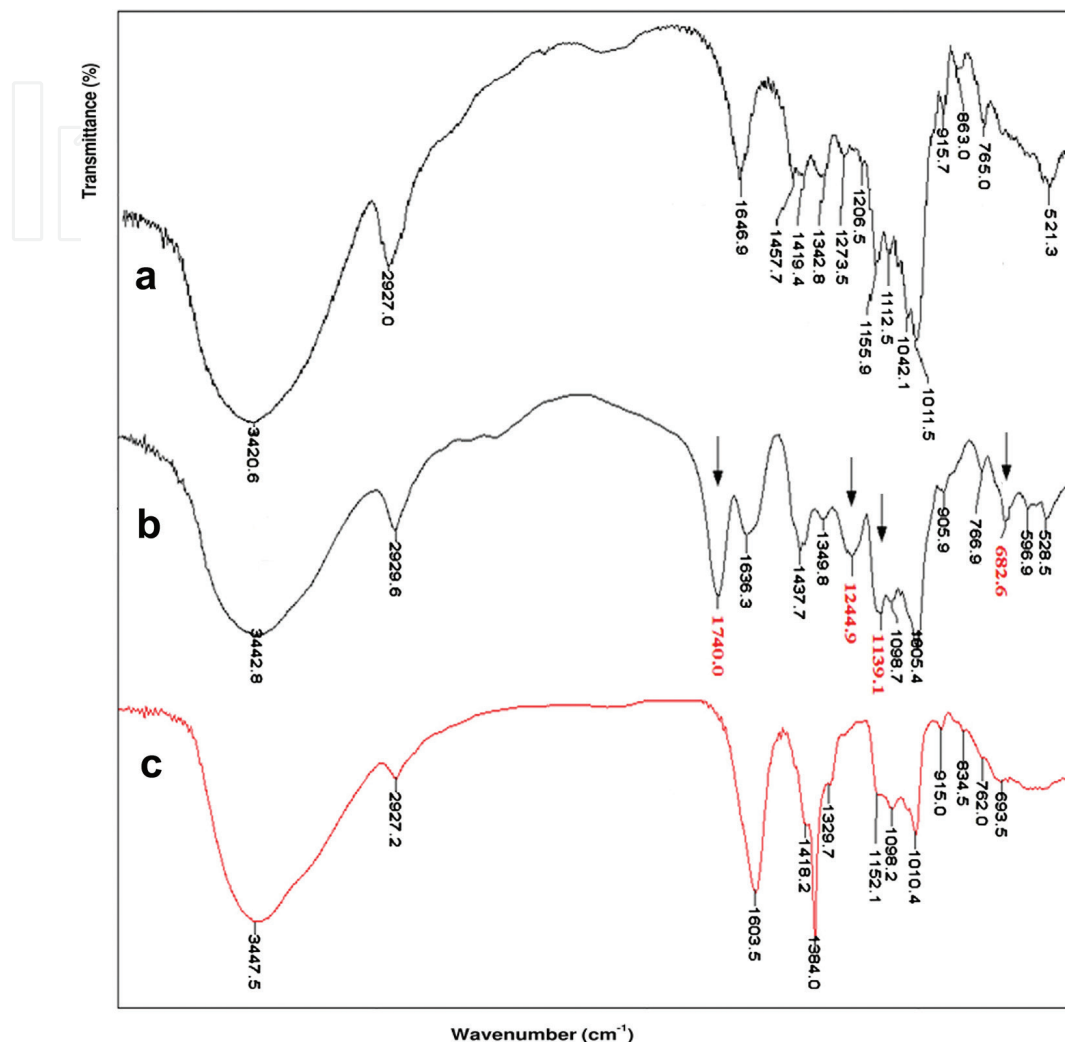


Figure 3. FTIR spectra of dextran (a), CMD (b), and AgNP-CMD (c).

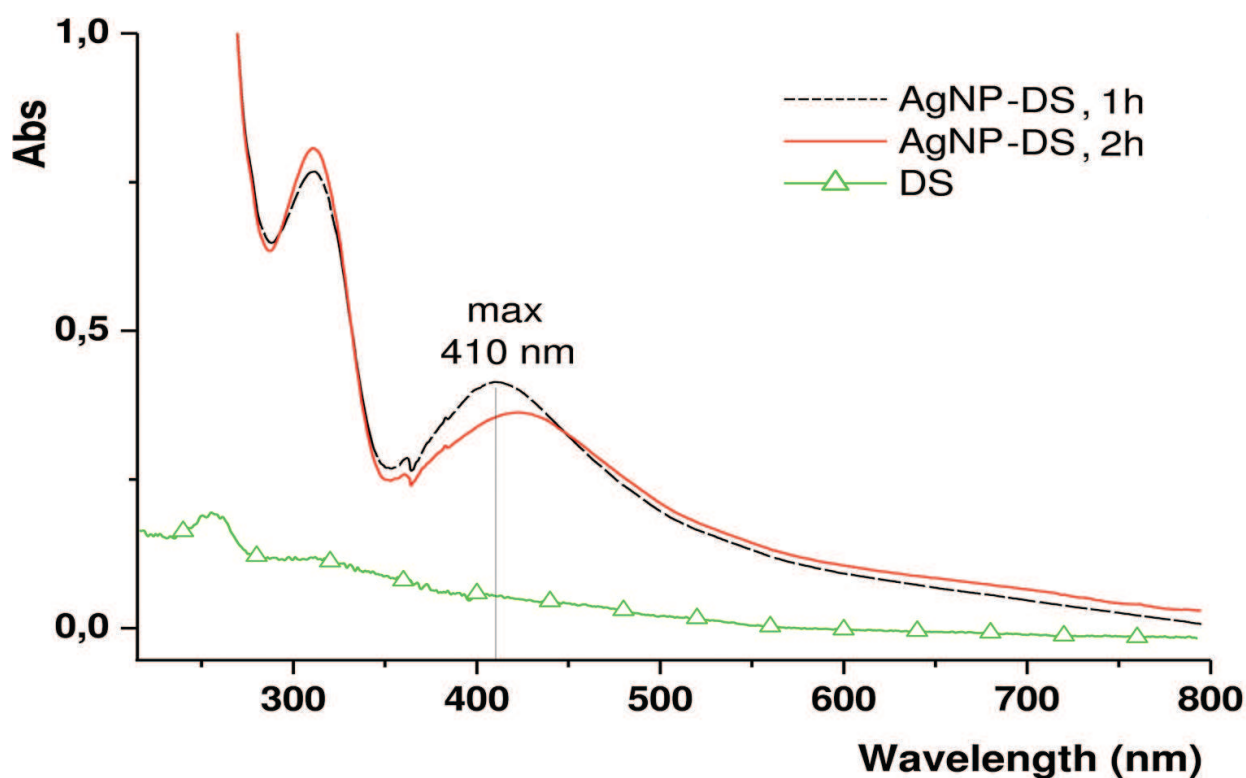
Assignment	DS (cm <sup>-1</sup> )	AgNP-DS (cm <sup>-1</sup> )	$\Delta\nu$ (cm <sup>-1</sup> )
$\nu_{\text{as}}$ (S-O)	1261	1239	22
$\nu_{\text{s}}$ (S-O)	988	1060	72
$\nu_{\text{as}}$ (O-S-O)	824	832	8
$\nu_{\text{s}}$ (O-S-O)	585	588	3
<sup>4</sup> C <sub>1</sub> conformation of the $\alpha$ -D-glucopyranose ring	915	915	–
	850	850	–
	745	752	7

Table 1. FTIR analysis data showing various functional groups present in dextran sulfate (DS) and AgNP-DS complex.

Speaking about carboxylate anion, delocalization of electrons causes the order of two CO bonds to be the same, so two bands (at 1600 and 1400  $\text{cm}^{-1}$ ) are expected in CO stretching vibration region, which are ascribed to asymmetric and symmetric C–O vibration, as it is indicated in the literature [13, 16, 28]. The similar situation is in AgNP-CMD complex (**Figure 3c**) in the CO groups vibration area. In fact, in this area of the spectrum, there are two intensive bands (at 1603 and 1420  $\text{cm}^{-1}$ ) which, according to its position and intensity should be attributed,  $\nu_{\text{as}}(\text{C-O})$  and  $\nu_{\text{s}}(\text{C-O})$  vibration, indicating coordination of  $\text{Ag}^+$  ions with a COOH group. In support of this is the absence of  $\nu(\text{C-O})$  and  $\delta(\text{C-OH})$  vibration bands. The appearance of spectrum in the area of 1000–700  $\text{cm}^{-1}$ , in all three tested compounds (**Figure 3**), is very similar and according to the literature data [30, 31] suggests  ${}^4\text{C}_1$  conformation of the glucopyranose unit.

### 2.3. UV-Vis study

Absorption spectra of starting ligand compounds (DSi CMD) as well as of final complexes (AgNP-DS and AgNP-CMD) are obtained by UV-Vis spectrophotometer (Varian Cary-100 Conc.). Spectrophotometric analysis was carried out in the range of 200–800 nm using original Cary UV-Conc. (Varian) software. The obtained UV-Vis spectra are presented in **Figures 4** and **5**.



**Figure 4.** UV-Vis spectra of dextran sulfate (DS) and AgNP-DS complex in function of the synthesis time.

Change in color from yellowish to brown, as well as careful interpretation of UV-Vis spectra, is used for estimating of AgNP synthesis [2–10]. A strong absorption band, called SPR band (surface plasmon resonance), is expected in 370–450 nm region in the UV-Vis spectrum of AgNP [32]. Its exact position depends on numerous factors (the most on AgNP size), while

intensity depends on their concentration [4, 21, 33]. Changes in this band position are used as a criterion of the AgNP stability, that is, aggregation of the nanoparticles during the time. As it can be seen from **Figure 4**, the existence of SPR band at 410 nm indicates the AgNP formation. However, its position is changed during synthesis with time, but after 2 h remains constant at 420 nm. The estimated particle size of AgNP-DS based on the UV data [34] is approximately 40 nm. A change in color from yellowish to brown during the synthesis has been observed in the case of AgNP-CMD formation. SPR band for this complex (**Figure 5**), synthesized at different molar ratio, is located at 420 nm, which is not present in the starting CMD. It is characteristic that intensity of this band is proportional to the amount of AgPN-CMD particles; it increases with increasing amounts of CMD, or during staying of the reaction mixture for 3 months (**Figure 5C**), which is similar to other studies [21]. Unchanged position of SPR band speaks in favor of good aggregation stability of synthesized particles. UV area below 300 nm was not investigated in the literature. However, in the UV spectra of tested compounds (**Figure 5**), there is an intense band of the formed complex at 215 nm ( $\pi \rightarrow \pi^*$  transition of the carboxyl group [35]) indicating red shift effect compared to CMD. This phenomenon is an indicator of Ag ions interaction with CMD and AgNP-CMD complex formation.

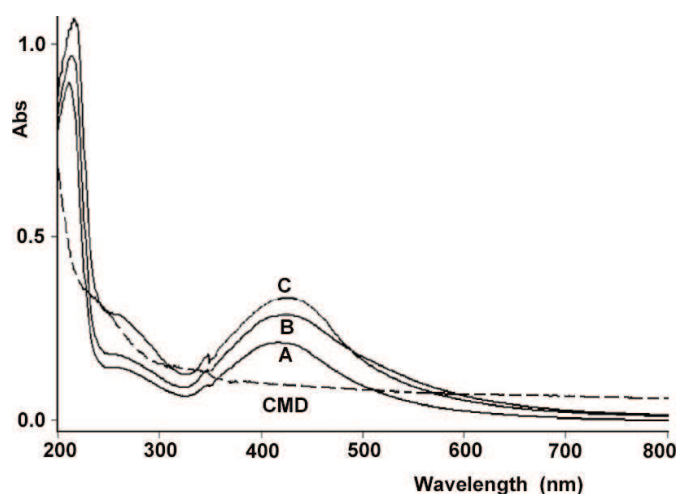


**Figure 5.** UV-Vis spectra of CMD ligand, AgNP-CMD = 1:1 complex (A), AgNP-CMD = 1:2 complex (B), and AgNP-CMD complex after 3 months (C).

## 2.4. XRD study

Crystal structure of AgNP-DS and AgNP-CMD nanoparticles was determined and confirmed by X-ray diffraction (XRD) technique. The samples were prepared by press and pull method in top-loading specimen plate [36]. The diffractogram was measured in Bragg-Brentano  $\theta$ :  $2\theta$  geometry by a conventional powder diffractometer, Seifert V-14, using Cu  $K\alpha$  radiation ( $\lambda_{Cu} K\alpha_1 = 1.5406 \text{ \AA}$ , Ni filter, generator settings: 30 kV, 30 mA). As an external standard for peak position calibration and instrumental peak broadening determination,  $LaB_6$  was used. XRD data were collected over the  $2\theta$  range of  $5\text{--}90^\circ$  with a step size of  $0.02^\circ$ , and an exposition time of 2 s per step. The obtained diffractograms are shown in **Figures 6 and 7**.

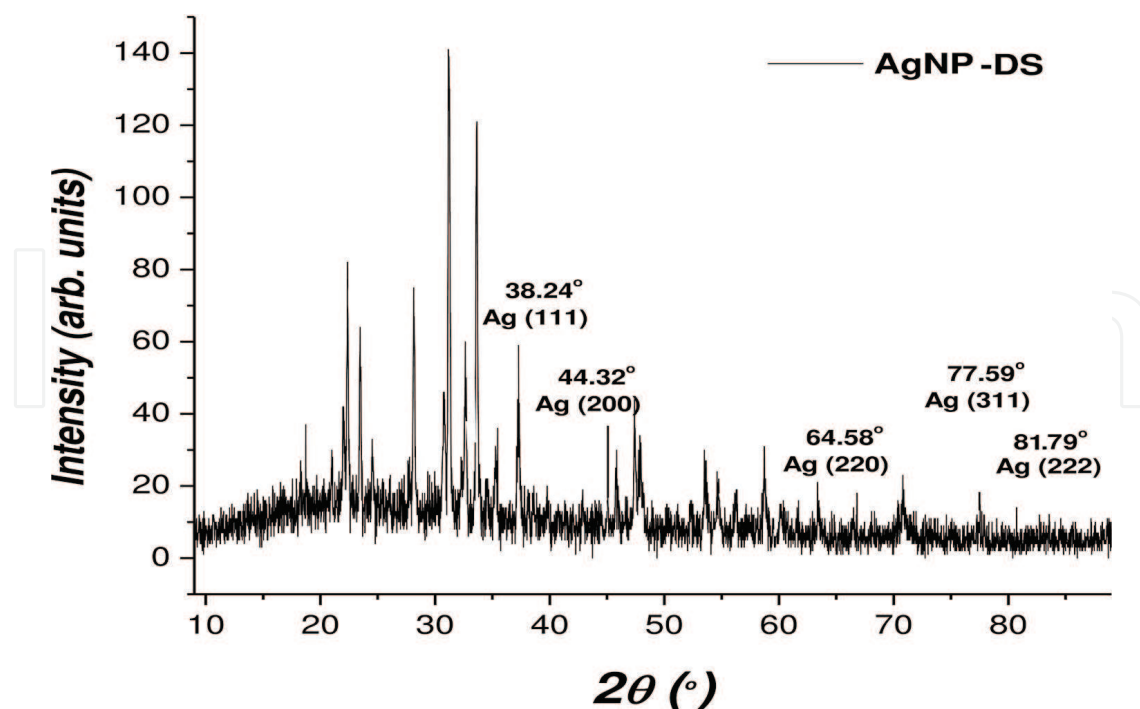


Figure 6. XRD diffraction patterns of AgNP-DS complex.

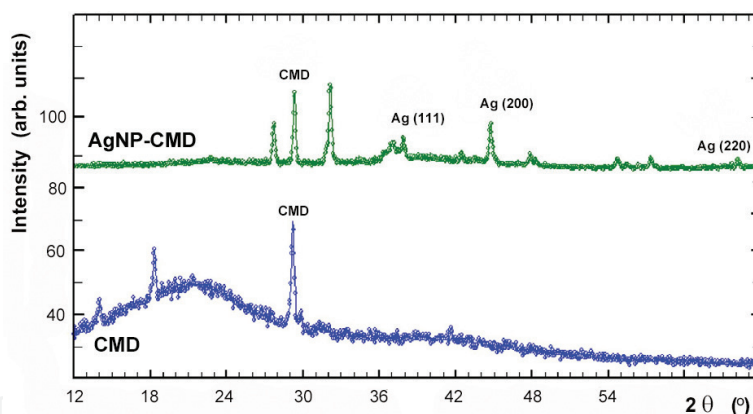


Figure 7. XRD diffraction patterns of CMD and AgNP-CMD complex.

From the presented X-ray diffraction patterns of AgNP-DS (**Figure 6**) can be noticed the XRD peaks at 38.24, 44.32, 64.58, 77.59, and 81.79°. Based on literature data [4, 6], the characteristic XRD peaks could be determined as next crystallographic planes: 111, 200, 220, 311, and 222. These planes are specific for the face-centered cubic silver crystals. This statement, along with the specified values, indicates the presence of silver nanoparticles in the synthesized AgNP-DS complex. Similar to the previous study, the crystal structure of Ag nanoparticles was determined with complex AgNP-CMD. Based on X-ray diffraction patterns (**Figure 7**) and the presence of XRD peaks at 38.02, 44.50, and 64.51°, a particular crystallographic planes are as follows: 111, 200, and 220, which are specific for the cubic silver crystals. According to literature [4, 6], the XRD peak at 29.01° is characteristic of the CMD ligand.

The calculation of average AgNP size has been done from the width of reflection in the X-ray diffraction pattern according to the Scherrer's equation (1):

$$D(2\theta) = K\lambda / FW_s \cos\theta \quad (1)$$

where  $D$  is the mean size of metal nanoparticles (nm);  $K$  is Scherrer constant (it's chosen 0.9—roughly spherical particles);  $\lambda$  is wavelength of X-ray radiation (nm);  $\theta$  is angle of diffraction ( $^\circ$ ); and  $FW_s$  is specimen broadening of single peak (in radians).  $FW_s$  is obtained according to the Eq. (2):

$$FW_s^d = FWHM^d - FW_1^d \quad (2)$$

where  $FWHM$  is full width at half maximum of the peak;  $FW_1$  is instrumental broadening gained from  $LaB_6$  diffractogram at the similar  $2\theta$  angles; and  $d$  is parameter of deconvolution (here  $d$  is chosen as 1.5 which means that shape is partly Gaussian and partly Lorentzian). According to Scherrer's equation (1) and XRD peak at  $38.24^\circ$   $2\theta$  from diffraction patterns (Figure 7), it is concluded that AgNP have mean crystallite size of  $40 \pm 4$  nm.

## 2.5. SEM and EDX study

The size and shape of AgNP-DS and AgNP-CMD complexes were further characterized by scanning electron microscopy (SEM) on JEOL JSM 5300 scanning electron microscope. Scanning micrographs were transformed into a PC format in order to further analyze the particles morphology. The samples for SEM analysis have been prepared by thin layer of the complex suspension overnight air drying at room temperature. Dried samples have been coated with 10-nm-thick film of gold in JPC JEOL-1100 apparatus. Electron beam of 30 keV has been used. The SEM micrographs of AgNP-DS (Figure 8A) showed both individual particles, but a number of aggregates, too. Size of 10–60 nm is predominant for individual spherical particles. Images have also indicated that obtained nanoparticles are stable, and they are not in a mutual contact. This can be ascribed to stabilization of the nanoparticles by DS as a capping agent. Aggregates of nanoparticles with poorly defined morphology and irregular structure have also been found (Figure 8A).

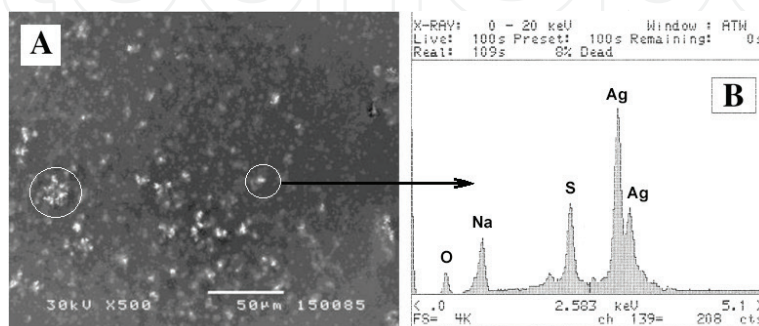


**Figure 8.** SEM images of AgNP-DS showing the existence of individual nanoparticle and large aggregates (A) and EDX spectrum of individual AgNP-DS (B.)

Energy-dispersive X-ray (EDX) spectral analysis has been performed by LINK Analytical 2000 QX microprobe assembled on a JEOL JSM 5300 scanning electron microscope. Samples prepared for SEM analyses have been used for EDX spectra measuring. EDX spectroscopy can be used for qualitative as well as quantitative assessment of silver used for the AgNP production [36]. EDX spectrum of AgNP-DS is shown in **Figure 8B**. Strong signal comes from elemental silver, while weaker signals come from S, O, and Na (from Na salt of DS), confirming that AgNP are formed as a part of AgNP-DS. This is consistent with an optical absorption peak appearance at approximately 3 eV (410 nm), which originates from SPR, and it is characteristic for metallic silver nanocrystals [6].

Similar to the previous complex, the SEM micrographs of AgNP-CMD (**Figure 9A**) show single particles, but a number of aggregates as well. Particle size of 10–60 nm is dominant for individual spherical particles. SEM images showed that obtained nanoparticles are stable and not in direct contact with each other. This can be explained as stabilization effect of CMD, as a capping agent, on produced nanoparticles. But, aggregated nanoparticles with larger irregular structure and no well-defined morphology were also found (**Figure 9B**).

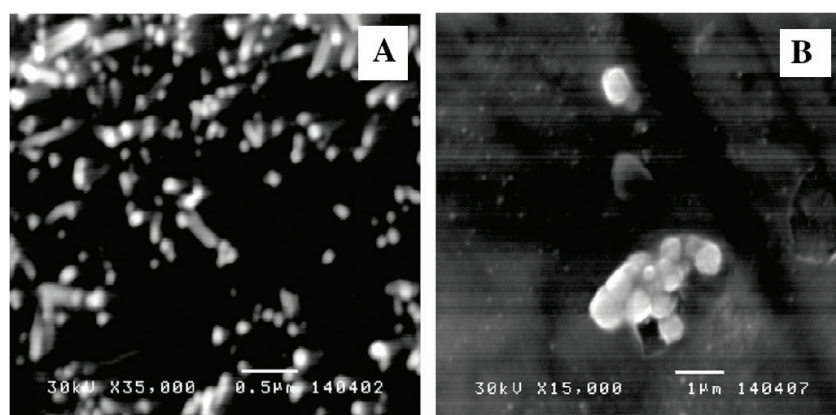


**Figure 9.** SEM images of individual spherical particles (A) and aggregated nanoparticles of AgNP-CMD (B).

## 2.6. Antimicrobial study

Agar disk diffusion method has been used for measuring of antibacterial and antifungal activity of AgNP stabilized by DS. One fungal strain (*Candida albicans* ATCC 2091) and nine bacterial strains such as Gram-positive (*Staphylococcus aureus* ATCC 25923, *Bacillus cereus* ATCC 11778, *Bacillus luteus* haus strain, *Bacillus subtilis* ATCC 6633, and *Listeria monocytogenes* ATCC 15313) and Gram-negative (*Escherichia coli* ATCC 25922, *Pseudomonas aeruginosa* ATCC 27853, *Klebsiella pneumoniae* ATCC 700603, and *Proteus vulgaris* ATCC 8427) were used as an indicator strain for this analysis. Preparation of suspension was performed by already described method [37]. Direct colony method has been used for bacterial and yeast suspensions preparation, and the colonies have been taken directly from the plate and suspended in 5 cm<sup>3</sup> of sterile 0.85% saline. Turbidity of the initial suspension has been adjusted comparing with 0.5 McFarland's [38]. After this adjustment, the bacterium and yeast suspensions contained close to 10<sup>8</sup> and 10<sup>6</sup> colony-forming units (CFU)/cm<sup>3</sup>, respec-

tively. Initial suspension has been additionally prepared by tenfold dilution into sterile 0.85% saline. Inoculation of bacterial cell suspensions has been done to the trypton soya agar plates, while the yeast suspension to the Sabouraud maltose agar plates. Standard sterile cellulose disks of 9 mm diameter have been impregnated with different AgNP-DS concentrations (0.25, 0.5, 1.0 mg cm<sup>-3</sup>) and putted on surface of the inoculated plates. The plates have been incubated at 37°C for 24 h. Inhibition zones were evaluated by measuring the diameter of the zones growth (**Table 2**).

Microbes		AgNP-DS concentration		
		0.25 mg cm <sup>-3</sup>	0.5 mg cm <sup>-3</sup>	1.0 mg cm <sup>-3</sup>
Fungi	<i>C. albicans</i>	–	16	–
Bacteria G <sup>+</sup>	<i>L. monocytogenes</i>	16	17	18
	<i>B. cereus</i>	16	18	19
	<i>B. subtilis</i>	16	17	19
	<i>S. aureus</i>	17	18	19
	<i>B. luteus haus strain</i>	20	21	24
Bacteria G <sup>-</sup>	<i>P. vulgaris</i>	13	14	15
	<i>K. pneumoniae</i>	16	18	19
	<i>E. coli</i>	17	18	21
	<i>P. aeruginosa</i>	23	24	26

**Table 2.** Antimicrobial activity of AgNP-DS, radial diameter of inhibition zones (mm) for tested bacterial and fungal strains.

The investigated AgNP-DS solution has shown antibacterial activity against *S. aureus*, *B. cereus*, *B. luteus in haus strain*, *B. subtilis*, *L. monocytogenes*, *E. coli*, *P. aeruginosa*, *K. pneumoniae*, and *P. vulgaris* bacteria, which is proved by clear inhibition zones of the bacteria growth around the disks (**Table 2**). Inhibition has been observed for all analyzed bacterial strains in the 0.25 mg cm<sup>-3</sup> concentration of AgNP-DS, indicating relatively low minimal inhibitory concentration against these microorganisms. For example, Dhand and coworkers [39] stated that minimal inhibitory concentrations for *E. coli* and *S. aureus* were around 0.26 mg cm<sup>-3</sup>. The highest inhibition zones were observed against *P. aeruginosa* and *B. luteus in haus strain*, and inhibition zones of AgNP-DS against these microorganisms in 1.0 mg cm<sup>-3</sup> concentration were 26 and 24 mm, respectively. *P. vulgaris* was the least sensitive to the AgNP-DS (1.0 mg cm<sup>-3</sup>) activity with zone of 15 mm. Investigation of AgNP-DS activity in different concentrations against other bacterial strains has shown similar results with inhibition zones of 16–17 mm, 18–19 mm, and 18–21 mm for the AgNP-DS concentration of 0.25, 0.5, and 1.0 mg cm<sup>-3</sup>, respectively. The results for *K. pneumoniae*, *B. luteus in haus strain*, and *P. aeruginosa* are higher compared to data for AgNP-CMD (**Table 3**). Antifungal activity against *C. albicans* was observed only in the concentration of 0.5 mg cm<sup>-3</sup> AgNP-DS. Low

antimicrobial activity of AgNP against *C. albicans* has been estimated for AgNP stabilized with CMD. The mechanism of AgNP antimicrobial activity can be related to silver accumulation in the membranes of bacteria, which cause cell death [40]. Silver cation can react with thiol groups and proteins in the cells; nonetheless, it can inactivate enzymes essential for the normal cell metabolism [41]. The investigated AgNP-DS particles, in the concentration of  $1.0 \text{ mg cm}^{-3}$ , have shown a number of specificity concerning its antimicrobial activity. It is important that higher concentration of silver is harmful for consumer and for microbes as well, so the lower concentrations are much more applicable. The effective concentrations of AgNP, which have effect in organisms different from the control, are in the range from a few  $\text{ng dm}^{-3}$  to  $10 \text{ mg dm}^{-3}$ ; this effective concentration is depended on the organism itself as well as many other factors [42]. Having in mind these results, it can be concluded that this design of silver nanoparticles synthesis has a great potential because of their antimicrobial activity.

Microbes		AgNP-CMD concentration		
		$0.25 \text{ mg cm}^{-3}$	$0.5 \text{ mg cm}^{-3}$	$1.0 \text{ mg cm}^{-3}$
Bacteria G <sup>+</sup>	<i>B. lutea</i>	11	13	20
	<i>B. cereus</i>	11	12	14
	<i>B. aureus</i>	12	18	21
Bacteria G <sup>-</sup>	<i>E. fecalis</i>	–	–	11
	<i>P. aeruginosa</i>	–	–	12
	<i>K. pneumoniae</i>	13	14	15
Fungi	<i>Aspergillus</i> spp.	–	–	12
	<i>Penicillium</i> spp.	13	20	20
	<i>C. albicans</i>	–	–	11

**Table 3.** Antimicrobial activity of AgNP-CMD, radial diameter of inhibition zones (mm) for tested bacterial and fungal strains.

In order to compare antimicrobial activity of similar complexes, the results of AgNP-CMD antimicrobial activity (radial diameter of inhibition zones) are presented in **Table 3**. The AgNP-CMD solution exhibited antibacterial activity against bacteria *B. lutea*, *B. aureus*, *B. cereus*, *E. fecalis*, *P. aeruginosa*, and *K. pneumoniae* showing clear inhibition zones of the bacteria growth around the disk. AgNP-CMD in the concentration of  $1.0 \text{ mg cm}^{-3}$  have shown a number of specificity concerning its antimicrobial activity. The antifungal activity of the AgNP-CMD has been analyzed by agar disk diffusion method. *Aspergillus* spp., *Penicillium* spp., and *C. albicans* were inhibited in a concentration-dependent manner. The radial growth inhibition zones increased with the AgNP-CMD concentration increasing from  $0.25$  to  $1.0 \text{ mg cm}^{-3}$ . The fungus *Penicillium* spp. was more sensitive to the AgNP-CMD comparing to the other two fungal strains.

### 3. Cobalt(II)-dextran biocomplexes

A lot of investigations in the field of coordination chemistry are based on synthesis and characterizations of different biocomplexes present in the biological systems. Synthetic ligands, which can serve as model molecules for complex biomolecular structures, are also investigated [19]. Bioligands or synthetic ligands are mostly natural macromolecular compounds. These products of special importance mostly represent complexes of different metals (Fe, Co, Cu, Zn) with ligands of polysaccharide type (such as pullulan, inulin, dextran) [43–45]. However, the native polysaccharide possessing antigen characteristics wherefore is not of pharmaceutical importance [18]. Depolymerization of raw polysaccharides, trying to get products with adequate molar masses distribution for commercial purposes, has been done. Dextran, is a well-known, extracellular, water-soluble neutral polysaccharide with  $\alpha$ -(1–6)-linked D-glucopyranose unit chain, with a wide range of applications. Dextran gained from *Leuconostoc mesenteroides* B-512(F) is composed of  $\alpha$ -(1–6)-linked glucan with side chains attached to C3-positions of backbone glucopyranose units. Various biometal ions (Fe, Co, Cu, Ca, Zn, Mg, etc.) are included in the complexation with dextran in alkaline solutions. Complexes of iron [17, 46] and copper [47–49] with polysaccharides have a great significance, and they have been described in detail. The content of metals and solution composition is pH dependent [17, 48]. Cobalt preparations, based on carbohydrates and its derivatives, are used in both human and veterinary medicine [50, 51]. The different FTIR spectroscopic methods (such as microspectroscopy, attenuated total reflection) are commonly used for the characterization of these complexes [52, 53]. This section applies to some spectroscopic examination of dextran complexes with cobalt ions.

#### 3.1. Complex synthesis

The cobalt complexes with reduced low-molar dextran as ligand (Co(II)-RLMD) were synthesized in water solutions, at different pH values (7.5–13.5) and different temperatures (298–373 K), using  $\text{CoCl}_2 \times 6\text{H}_2\text{O}$  and RLMD (5000 g/mol). The details of synthesis have been described [54, 55]. The complexes were isolated in the solid state. For further structural examination, the samples of Co(II)-RLMD were deuterated ( $\text{D}_2\text{O}$ , Merck) for 2 h, at room temperature, in vacuum.

#### 3.2. FTIR study

KBr pastille method has been used for sample preparation. The FTIR spectra have been recorded at room temperature, as an average value of 40 scans (resolution of  $2\text{ cm}^{-1}$ ) on a Bomem MB-100 FTIR spectrometer (Hartmann & Braun, Canada) coupled with a DTGS/KBr detector. Spectro-structural correlation of dextran by FTIR spectroscopy has been the subject of attention of many researchers [30, 31, 56–58]. It was shown that by studying the individual spectral areas, the information on linearity [content of  $\alpha$ -(1–6) bond], crystallinity, conformation, conformational transitions, and changes in the structure of differently treated dextrans can be obtained. The FTIR spectrum of reduced low-molar dextran is shown in **Figure 11a**. Bands at 765 and  $916\text{ cm}^{-1}$  are indicating the presence of the  $\alpha$ -(1–6) glycosidic bonds, and the estimated content of these bonds is greater than 96% that indicates a high linearity of polysaccharide. The presence of these bands as those at the  $845\text{ cm}^{-1}$  indicates a  $\text{C}_1$  conformation of glucopyranose units

(eq-ax-ax-ax-ax arrangement of adjacent C–H groups). There is an intense broad band whose centroid is at about  $3400\text{ cm}^{-1}$ , in the area of stretching OH vibrations. Summary intensity of this band comes from the  $\nu(\text{O-H})$  vibrations of hydroxyl groups involved in the formation of several by the strength of hydrogen bonds, but also from the  $\text{H}_2\text{O}$  molecule whose presence is confirmed by the band at  $1640\text{ cm}^{-1}$ , which is result of  $\delta(\text{HOH})$  vibrations [54].

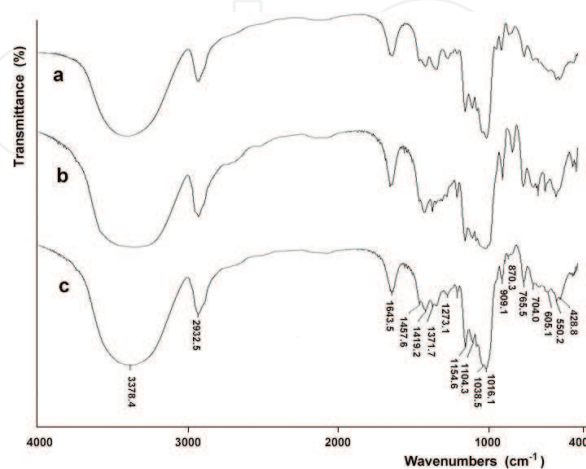


**Figure 10.** The FTIR spectra of RLMD (a) and Co(II)-RLMD complexes synthesized on the boiling temperature and different pH: 7.5 (b) and 13.0 (c).

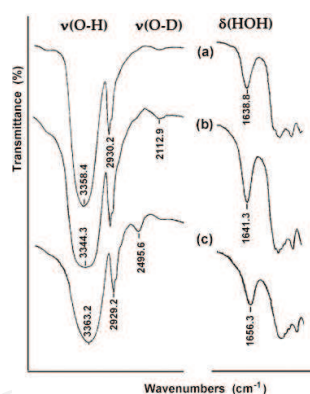


**Figure 11.** FTIR spectral segments of dextran (a), partially deuterated (b), and fully deuterated (c) RLMD analogs in  $\nu(\text{O-H})$ ,  $\nu(\text{O-D})$ , and  $\delta(\text{HOH})$  vibrations.

The FTIR spectra of synthesized Co(II)-RLMD complex, which were obtained under various reaction conditions, are presented in **Figure 10**. The FTIR spectra of RLMD and its Co(II)-RLMD complex are basically similar. In the FTIR spectra of synthesized complex, there are the differences in the area of O–H vibrations. In this area, there is a large, complex band approximately  $3390\text{ cm}^{-1}$  of  $\nu(\text{O-H})$ , which is likely due to the stretching vibrations of polysaccharide OH groups. The characteristic IR band of  $\delta(\text{HOH})$  at about  $1645\text{ cm}^{-1}$  in the spectra of synthesized complexes, as well as in the spectrum of RLMD, as noted above, indicates the presence of crystal water in the structure [54, 55]. By analyzing the low-frequency part of the RLMD spectrum ( $\gamma(\text{C-H})$  vibrations, **Figure 10a**), the FTIR spectra of Co(II)-RLMD complex

(**Figure 10b** and **c**), and the presence of bands at about 915 and 845  $\text{cm}^{-1}$ ,  ${}^4\text{C}_1$  conformation of glucopyranose units, which indicates that the complexation with Co(II) ions does not lead to conformational changes in glucopyranose units, can be determined. In accordance with this is the change in the intensity of IR band in the area approximately 1350  $\text{cm}^{-1}$  that originates from  $\delta(\text{C-H})$  and  $\delta(\text{O-H})$  vibrations. With an increase in the pH synthesis (from 7.5 to 13.5), the band intensity of  $\nu(\text{O-H})$  vibration increases, and the frequency of  $\nu(\text{O-H})$  vibration band at lower pH (7.5–8.5) stays almost unchanged and then increases with increasing pH (11–13.5). If the complexation with Co(II) ions takes place via OH groups at the C-2, C-3, or C-4 carbon atoms of dextran glucopyranose units (involved in the formation of various by the strength of hydrogen bonds in dextran), hydrogen bonds disappear by complexation, so the bands are expected at the higher frequencies. In complexes with the highest metal content (10.07% Co), which were synthesized at pH 12, a set of IR bands in this area is close to that at starting RLMD. In the complex which was synthesized at pH 13 with a minimum cobalt content of 1.89% in the IR spectrum (**Figure 10c**), there are intense bands at 3400  $\text{cm}^{-1}$  to the binder of low-frequency side in this region. This could indicate that the structure of this complex differs slightly from the structure of other Co(II)-RLMD complex, which were synthesized under different reaction conditions. In the low-frequency area ( $<800 \text{ cm}^{-1}$ ) of the FTIR spectra of RLMD and Co(II)-RLMD complex, there are some differences. In this region of the IR spectrum, in addition to the band of  $\nu(\text{Co-O})$ , the bands of deformation  $\gamma(\text{O-H})$  vibrations of polysaccharide as well as the deformation vibrations of glucopyranose ring are expected (**Figure 10**). Wide band of medium intensity in the FTIR spectra of Co(II)-RLMD complex at about 450  $\text{cm}^{-1}$  shows a fine structure.

### 3.3. Isotopic $\text{D}_2\text{O}$ exchange study

Isotopic substitution of hydrogen atoms by deuterium, connected with FTIR spectroscopy, has an important role in determining the structure of dextran. Isotopic exchange results indicate that dextran and its Co(II)-RLMD complex are crystal hydrates (probably one type of water molecules) [59]. Structural changes in the process have been detected by absorption bands in the area of 3600–3000  $\text{cm}^{-1}$ , caused by  $\nu(\text{O-H})$  vibrations. In the case of isotopic exchanges of O-H to O-D group, the frequency of stretching vibration is reduced to  $\sqrt{2}$ , and it is located in the area of 2700–2300  $\text{cm}^{-1}$ . Deuteration is a very sensitive method to assess the environment of OH groups, which is associated with the intensity generated by hydrogen bonds. The degree of crystallinity of the polysaccharide can be determined by FTIR spectroscopy method with deuteration. Crystallinity is a part of the regulated saccharide area in which the macromolecules are connected with parallel hydrogen bonds. In processing the sample with  $\text{D}_2\text{O}$ , usually OH groups in less regulated or amorphous regions were rapidly converted into OD groups. Conversion of OH groups in the crystal areas is very slow. Thus, the degree of crystallinity has been determined by the change in intensity of asymmetrical  $\nu(\text{O-H})$  band vibrations and by the appearance of new bands of  $\nu(\text{O-D})$  vibration. The relations of band intensity at 1429 and 893  $\text{cm}^{-1}$  were taken as empirical indicators of the degree of crystallinity of samples. With decrease in the crystallinity, the band at about 1430  $\text{cm}^{-1}$  disappears and comes to an increase in the intensity of the band at approximately 900  $\text{cm}^{-1}$ , typical for the amorphousness. Even better relationship can be seen at the band at approximately 1370 and 2900  $\text{cm}^{-1}$ . Namely, in the spectrum of partially deuterated analogs of dextran (**Figure 11**) in

the  $\nu(\text{O-D})$  area of the vibration of HDO molecules, there is a single band at about  $2495\text{ cm}^{-1}$ . Partners of these vibrations would be expected at about  $3400\text{ cm}^{-1}$  in the  $\nu(\text{O-H})$  areas (taking into account the displacement factor of 1.35).

The FTIR spectra of Co(II)-RLMD complex (a) and its deuterated analog (b), which was synthesized at pH 13, are shown in **Figure 12**. In the FTIR spectrum of Co(II)-RLMD complex (**Figure 12b**), in the area of  $\nu(\text{O-D})$  vibrations of HDO molecules, there is a single band at about  $2483\text{ cm}^{-1}$  in the corresponding complexes with crossfold on the high-frequency side. Partners of these vibrations would be expected at about  $3400\text{ cm}^{-1}$  in  $\nu(\text{O-H})$  area. Results of partial deuteration indicate that the band at about  $3400\text{ cm}^{-1}$  is sensitive to isotopic substitution, in both cases (RLMD and Co(II)-RLMD complexes). Reducing the intensity of this band by deuteration demonstrates that the  $\nu(\text{O-H})$  vibrations of water molecules are its part. This fact indicates that both compounds contain crystal water in their structure. Confirmation of this conclusion is that in the spectra of deuterated analogs of both compounds (**Figures 11 and 12**), an intense band near  $1645\text{ cm}^{-1}$  is also highly sensitive to isotopic substitution and is to be attributed to the HOH deformation vibration of the crystal water.

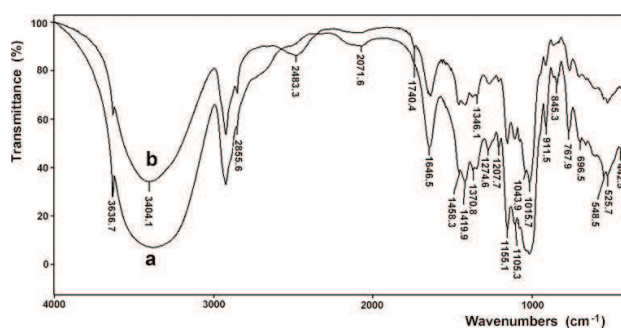


**Figure 12.** FTIR spectra of Co(II)-RLMD complex (a) and its deuterated analog (b) synthesized at pH 13.

As known, Seidl et al. [60] proposed criteria according to which, based on the study of spectra of protonated, partially and fully deuterated hydrate, it is possible to determine the number of types of  $\text{H}_2\text{O}$  molecules ( $n$ ) and the number of nonequivalent OH groups ( $m$ ). By the spectra appearances, in the stretching OD area of HDO molecules, and the appearance of a band, whose intensity increases monotonically with increasing degree of deuteration when the frequency does not change, it can be concluded from the above criteria [60] that in the structure of dextran and its complexes with Co(II) ions is present one crystallographic type of water molecule ( $n = 1$ ). On the basis of Berglund correlation [61], from equation (3), Ow...O distances are estimated at 283.1 pm for dextran and 281.8 pm for Co(II)-RLMD complex:

$$\nu(\text{OD}) = 2727 - 8.97 \times 10^6 \times e^{-3.73 \times R(\text{Ow} \times \times \text{O})}. \quad (3)$$

Water protons are involved in the formation of relatively weak hydrogen bonds ( $m = 1$ ). In bending area of HDO and  $\text{D}_2\text{O}$ , in the spectrum of deuterated analogs of the complex, there are bands around  $1315$  and  $1070\text{ cm}^{-1}$ , which confirm the previously disclosed consideration

of the water binding. From FTIR spectrum shown in **Figure 12b**, decrease in the intensity of the band around  $1430\text{ cm}^{-1}$  and an increase in the band intensity at approximately  $910\text{ cm}^{-1}$  can be observed, which is a characteristic for amorphous character. An even better relationship can be observed in the FTIR spectrum of **Figure 12**, with the band of about  $1370$  and  $2900\text{ cm}^{-1}$ . Based on the results of FTIR spectroscopy, an amorphous structure of the synthesized Co(II)-RLMD complex can be assumed.

### 3.4. ATR-FTIR microscopy study

The ATR-FTIR spectral analysis has been performed by microspectroscopy ATR-FTIR system (Bruker, Tensor-27). Within this system, FTIR spectroscope is connected to a microscope ( $15\times$  objective) (Bruker, Hyperion-1000/2000) and a computer system capable of microanalysis by using a liquid-nitrogen-cooled ( $250\text{ }\mu\text{m}$ ) MCT detector (GMBH, Germany). The ATR-FTIR spectra (Kubelka-Munk option) have been recorded in the range of  $4000\text{--}400\text{ cm}^{-1}$ , with  $4\text{ cm}^{-1}$  resolution and 260 scans. The newly formed FTIR vibrational microspectroscopy can provide information on the sample at the molecular level, with high spatial resolution at the microscopic level. Small sample can be analyzed by both nondestructive vibrational spectroscopic techniques (Raman, IR) [62–67]. Spectra can be recorded continuously in different parts of the microsample in order to obtain appropriate databases. **Figures 13** and **14** show the absorption ATR-FTIR spectra of Co(II)-RLMD complex, which were obtained under various reaction conditions.

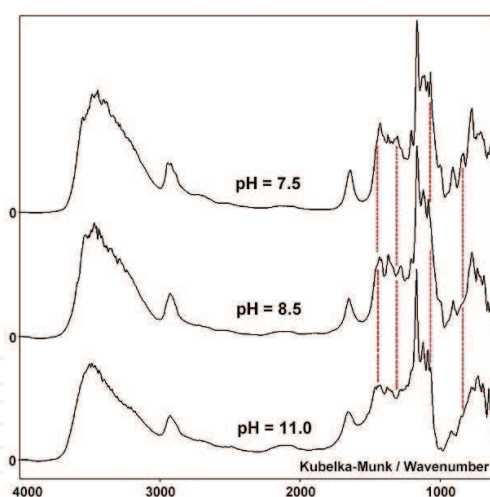


**Figure 13.** ATR-FTIR spectra of Co(II)-RLMD complex synthesized at the boiling temperature and pH values in the range of 7–11.

The wavenumber values of characteristic IR bands in the ATR-FTIR spectra of Co(II)-RLMD complex are given in **Table 4**.

Absorption bands corresponding to the specific chemical components can be represented as a map. ATR-FTIR spectra, presented in **Figures 13** and **14**, correspond to the different

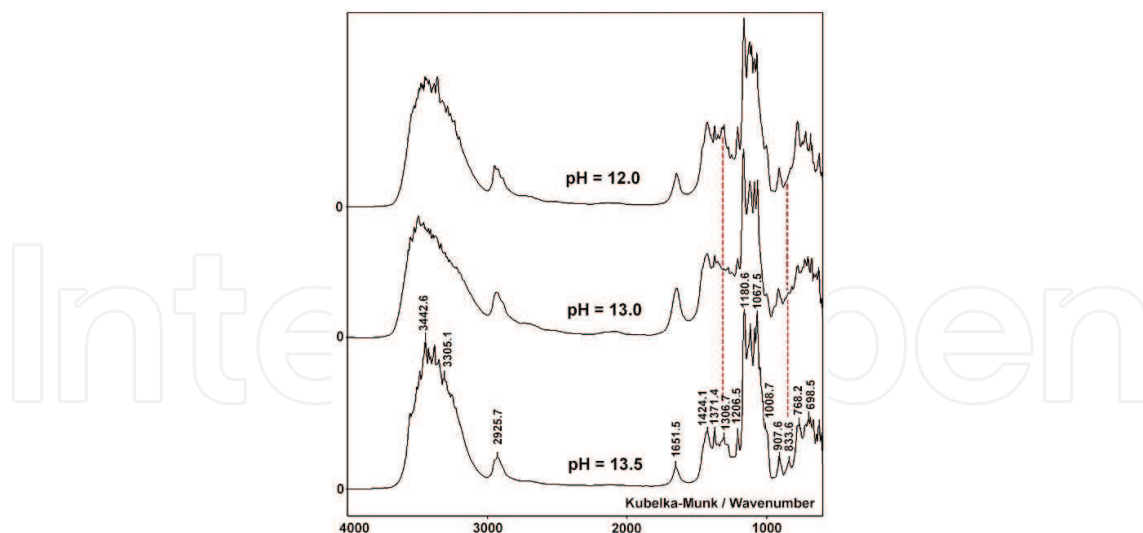


**Figure 14.** ATR-FTIR spectra of Co(II)-RLMD complex synthesized at the boiling temperature and pH values in the range of 12–14.

Wavenumber (cm <sup>-1</sup> )	Band assignment	Intensity	Comment
3400	$\nu(\text{O-H})$	Very strong, complex	CH-OH glucopyranose, H <sub>2</sub> O
2930	$\nu_{\text{as}}(\text{C-H})$ i $\nu_{\text{sy}}(\text{C-H})$	Medium	CH
1640	$\delta(\text{HOH})$	Medium	H <sub>2</sub> O
1450–1345	$\delta(\text{C-H})$	Medium	CH
1420	$\delta(\text{O-H})$	Medium	OH
1150, 1110, 1070, 1040, and 1010	$\nu_{\text{as}}(\text{C-O}), (\text{C-O-C}),$ $\nu_{\text{as}}(\text{C-C-C})$ i $(\text{C-C-O})$	Very strong, strong	Glucopyranose
1000–700	$\gamma(\text{C-H})$	Medium	Configuration

**Table 4.** Assignment of characteristic IR bands of RLMD and the synthesized Co(II)-RLMD complexes.

parts of the sample of Co(II)-RLMD complex, which show a homogeneity of the samples. A new way of visualization shows the capability of visualization not only of heterogeneous region of the samples, but also at the same time provides microspectroscopic spatial information. The visualization of different concentrations of components and presentation as 3D maps is also enabled. Application of ATR-FTIR microscopy to Co(II)-RLMD complex, which were synthesized under different reaction conditions, is shown in **Figure 15**. The changes in color contours at certain parts of the image indicate the content and distribution of cobalt and polysaccharides in Co(II)-RLMD samples. ATR-FTIR microspectroscopic data show a high homogeneity of the samples, and the presence of Co(II) ions (the results obtained by other spectroscopic techniques) has been confirmed by the color of Co(II)-RLMD complex.

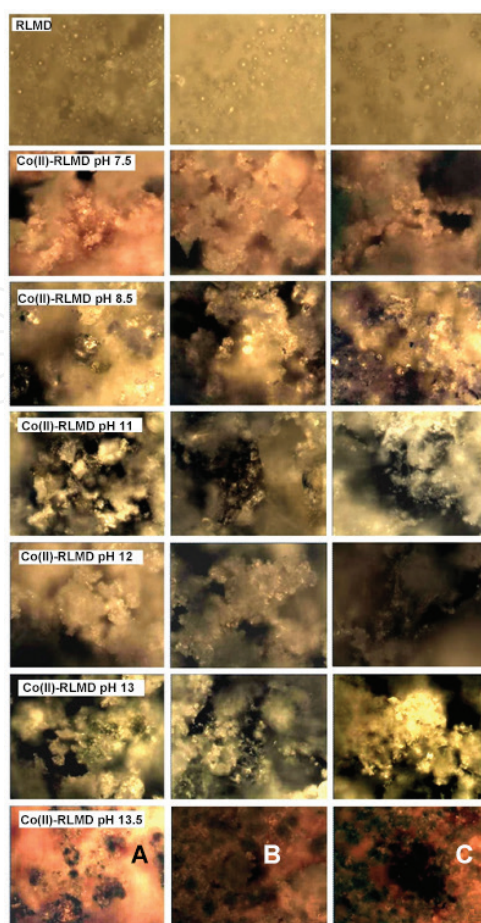


**Figure 15.** Different FTIR microscopic profiles (A–C) ( $300\ \mu\text{m} \times 250\ \mu\text{m}$ ) for ligand (RLMD) and Co(II)-RLMD complexes at different pH values.

#### 4. Conclusion

The modern Fourier transform infrared spectroscopic techniques (linear scan, reflection, transmission, mapping, video analysis) in combination with diffraction (XRD), energy-dispersive X-ray (EDX), spectrophotometric (UV-Vis), and electronic microscopy (SEM) methods are applied in the structure analysis of synthesized green nanoparticles and polysaccharide complexes, as well as for the confirmation of suggested types of complexes structure and for the testing of samples homogeneity. In this respect, silver nanoparticles were prepared with dextran sulfate or carboxymethyl dextran as a reducing and capping agent, while cobalt biocomplexes were synthesized with reduced low-molar dextran as ligand. Comparison of FTIR spectra of initial exopolysaccharide compounds (DS, CMD, RLMD) and final products (AgNP-DS, AgNP-CMD, Co(II)-RLMD complexes), in the specific region of characteristic functional group vibrations, has indicated on coordination complexes forming as a part of complex structure. FTIR spectroscopic analysis has shown that interactions between metal ions and specific polysaccharide functional groups have steric character and suggest  ${}^4C_1$  conformation of the glucopyranose unit. The existence of nanoparticles (in range of 10–60 nm) has been confirmed by SPR band in the UV-Vis spectra, by SEM microscopy, and XRD meth-

ods. AgNP size was determined on the Bragg reflection at  $38.24^{\circ}2\theta$ , yielding mean crystallite size of  $40 \pm 4$  nm. It has been found that crystalline structures of silver complexes are face-centered cubic type by XRD method. Morphological SEM analysis has been shown that formed nanoparticles are spherical and inclined to aggregation. It has been established that size distribution and morphology of mentioned nanoparticles (by SEM and FTIR microspectroscopy methods), as well as the structural form of the complexes (by FTIR, UV-Vis, XRD), are depended on ligand properties (such as constitution, degree of amorphousness or crystallinity, molar mass, units conformation, chain linearity) and on the reaction conditions (such as metal-ligand weight ratio, reaction time, temperature, and pH values). Also, antimicrobial and antifungal activities of synthesized AgNP have been determined. The highest inhibition zones were observed against *P. aeruginosa* and *B. luteus* strain, while *P. vulgaris* was the least sensitive to the nanoparticles. The fungus *Penicillium* spp. was more sensitive to the AgNP comparing to the other two fungal strains. Having in mind these results, it can be concluded that this design of silver nanoparticles synthesis has a great potential because of their antimicrobial activity.

## Acknowledgements

This study is the result of the project TR-34012, funded by the Ministry of Education, Science and Technological Development, of the Republic of Serbia.

## Author details

Goran S. Nikolić<sup>1\*</sup>, Milorad D. Cakić<sup>1</sup>, Slobodan Glišić<sup>1</sup>, Dragan J. Cvetković<sup>1</sup>, Žarko J. Mitić<sup>2</sup> and Dragana Z. Marković<sup>3</sup>

\*Address all correspondence to: [goranchem\\_yu@yahoo.com](mailto:goranchem_yu@yahoo.com)

1 Department of Chemical Technology, Faculty of Technology, University of Niš, Leskovac, Serbia

2 Department of Chemistry, Faculty of Medicine, University of Niš, Niš, Serbia

3 High Technologically Artistic Professional School, Leskovac, Serbia

## References

- [1] A.L. Daniel-da-Silva, T. Trinidad, Biofunctional composites of polysaccharides containing inorganic nanoparticles, *Adv. Nanotechnol.* 98(7) (2011) 953–955. ISBN 978-953-308-55-0
- [2] P.V. Quelemes, F.B. Araruna, B.E.F. de Faria, S.A.S. Kuckelhaus, D.A. da Silva, R.Z. Mendonça, C. Eiras, M.S. Soares, J.S.A. Leite, Development and antibacterial activity of cashew gum-based silver nanoparticles, *Int. J. Mol. Sci.* 14 (2013) 4969–4981.

- [3] H.V. Tran, L.D. Tran, T.B. Cham, H.D. Vu, T.N. Nguyen, D.G. Pham, P.X. Nguyen, Synthesis, characterization, antibacterial and antiproliferative activities of monodisperse chitosan-based silver nanoparticles, *Colloids Surf. A* 360 (2010) 32–40.
- [4] P. Kanmani, S.T. Lim, Synthesis and characterization of pullulan-mediated silver nanoparticles and its antimicrobial activities, *Carbohydr. Polym.* 97 (2013) 421–428.
- [5] M.B. Ahmad, J.J. Lim, K. Shamel, N.A. Ibrahim, M.Y. Tay, Synthesis of silver nanoparticles in chitosan, gelatin and chitosan/gelatin bionanocomposites by a chemical reducing agent and their characterization, *Molecules* 16 (2011) 7237–7248.
- [6] K.P. Bankura, D. Maity, M.M.R. Mollick, D. Mondal, B. Bhowmick, M.K. Bain, A. Chakraborty, J. Sarkar, K. Acharya, D. Chattopadhyay, Synthesis, characterization and antimicrobial activity of dextran stabilized silver nanoparticles in aqueous medium, *Carbohydr. Polym.* 89 (2012) 1159–1165.
- [7] D. Chudobova, K. Cihalova, B. Ruttkay-Nedecky, P. Kopel, M. Zurek, K. Bastl, V. Adam, R. Kizek, Use of the silver phosphate nanoparticles (SPNPs) for their antimicrobial effect on bacterial strains, *Nanocon 16–18.10.2013, Brno, Czech Republic, EU* (2013).
- [8] D. Chudobova, L. Nejd, J. Gumulec, O. Krystofova, M.A.M. Rodrigo, J. Kynicky, B. Ruttkay–Nedecky, P. Kopel, P. Babula, V. Adam, R. Kizek, Complexes of silver(I) ions and silver phosphate nanoparticles with hyaluronic acid and/or chitosan as promising antimicrobial agents for vascular grafts, *Int. J. Mol. Sci.* 14 (2013) 13592–13614.
- [9] S.M. Ghaseminezhad, S. Hamedi, S.A. Shojaosadati, Green synthesis of silver nanoparticles by a novel method: comparative study of their properties, *Carbohydr. Polym.* 89 (2012) 467–472.
- [10] M.N. Nadagouda, R.S. Varma, Synthesis of thermally stable carboxymethyl cellulose/metal biodegradable nanocomposites for potential biological applications, *Biomacromolecules* 8(9) (2007) 2762–2767.
- [11] J. Liu, F. He, T.M. Gunn, D. Zhao, C.B. Roberts, Precise seed-mediated growth and size-controlled synthesis of palladium nanoparticles using a green chemistry approach, *Langmuir* 25(12) (2009) 7116–7128.
- [12] F. He, D. Zhao, J. Liu, C.B. Roberts, Stabilization of Fe-Pd nanoparticles with sodium carboxymethyl cellulose for enhanced transport and dechlorination of trichloroethylene in soil and groundwater, *Ind. Eng. Chem. Res.* 46(1) (2007) 29–34.
- [13] M.A. Garza-Navarro, J.A. Aguirre-Rosales, E.E. Llanas-Vazquez, I.E. Moreno-Cortez, A. Torres-Castro, V. Gonzalez-Gonzalez, Totally ecofriendly synthesis of silver nanoparticles from aqueous dissolutions of polysaccharides, *Int. J. Polym. Sci.* 2013 (2013) 436201. 8 pages. doi:10.1155/2013/436021
- [14] E.M. Prinz, R. Eggers, H.H. Lee, U. Steinfeld, R. Hempelmann, Synthesis of drug loaded magnetic nanoparticles and their uptake into immune cells, *J. Phys. Conf. Ser.* 200 (2010) 122009. doi:10.1088/1742-6596/200/12/122009

- [15] K. Tao, S. Song, J. Ding, H. Dou, K. Sun, Carbonyl groups anchoring for the water dispersibility of magnetite nanoparticles, *Colloid Polym. Sci.* 289 (2011) 361–369.
- [16] A.M. Abdel-Mohsen, R. Hrdina, L. Burgert, G. Krylova, R.M. Abdel-Rahman, A. Krejcová, M. Steinhart, L. Benes, Green synthesis of hyaluronan fibers with silver nanoparticles, *Carbohydr. Polym.* 89 (2012) 411–422.
- [17] G.S. Nikolić, M. Cakić, Lj. Ilić, S. Ristić, Ž. Cakić, Synthesis of some new antianemics I. Iron pullulan complexes of pharmaceutical interest, *Pharmazie* 57(3) (2002) 155–158.
- [18] O. Elmalak, M.A. Lovich, E. Edelman, Correlation of transarterial transport of various dextrans with their physicochemical properties, *Biomaterials* 21 (2000) 2263–2272.
- [19] B. Gyurcsik, L. Nagy, Carbohydrates as ligands: coordination equilibria and structure of the metal complexes, *Coord. Chem. Rev.* 203 (2000) 81–149.
- [20] D. Wei, W. Sun, W. Qian, Y. Ye, X. Ma, The synthesis of chitosan-based silver nanoparticles and their antibacterial activity, *Carbohydr. Res.* 344 (2009) 2375–2382.
- [21] S. Hamed, S.M. Ghaseminezhad, S.A. Shojaosadati, S. Shokrollahzadeh, Comparative study on silver nanoparticles properties produced by green methods, *Iran. J. Biotechnol.* 10 (2012) 191–197.
- [22] S. Glišić, M. Cakić, G.S. Nikolić, B. Danilović, Synthesis, characterization and antimicrobial activity of carboxymethyl dextrane stabilized silver nanoparticles, *J. Mol. Str.* 1084 (2015) 345–351.
- [23] S. Tripathi, G.K. Mehrotra, P.K. Dutta, Chitosan silver oxide nanocomposite film: preparation and antimicrobial activity, *Bull. Mater. Sci.* 34(1) (2011) 29–35.
- [24] M. Guzman, J. Dille, S. Godet, Synthesis and antibacterial activity of silver nanoparticles against gram-positive and gram-negative bacteria, *Nanomedicine* 8(1) (2012) 37–45.
- [25] S. Glišić, G.S. Nikolić, M. Cakić, N. Trutić, Spectroscopic study of copper(II) complexes with carboxymethyl dextran and dextran sulphate, *Russ. J. Phys. Chem. A* 89(7) (2015) 1254–1262.
- [26] M. Cakić, G.S. Nikolić, Lj. Ilić, S. Stanković, Synthesis and FTIR characterization of some dextran sulphates, *Chem. Ind. Chem. Eng. Q* 11(2) (2005) 74–78.
- [27] V.A. Litvin, B.F. Minaev, Spectroscopy study of silver nanoparticles fabrication using synthetic humic substances and their antimicrobial activity, *Spectrochim. Acta Part A Mol. Biomol. Spectrosc.* 108 (2013) 115–122.
- [28] A.L. Daniel-da-Silva, S. Fateixa, A.J. Guiomar, B.F.O. Costa, N.J.O. Silva, T. Trindade, B.J. Goodfellow, A.M. Gil, Biofunctionalized magnetic hydrogel nanospheres of magnetite and  $\kappa$ -carrageenan, *Nanotechnology* 20(35) (2009) 355602. doi:10.1088/0957-4484/20/35/355602
- [29] X.F. Bao, Y. Zhen, L. Ruan, J.N. Fang, Purification, characterization, and modification of T lymphocyte-stimulating polysaccharide from spores of *Ganoderma lucidum*, *Chem. Pharm. Bull. (Tokyo)* 50 (2002) 623–629.

- [30] R.G. Zhabankov, *Infrared spectra and structure of carbohydrates*, Nauka i Tekhnika, Minsk, Belarus, 1972.
- [31] V.P. Panov, R.G. Zhabankov, *Intra- and intermolecular interactions in carbohydrates*, Nauka i Tekhnika, Minsk, Belarus, 1988.
- [32] M.R. Bindhu, M. Umadevi, Synthesis of monodispersed silver nanoparticles using *Hibiscus cannabinus* leaf extract and its antimicrobial activity, *Spectrochim. Acta Part A Mol. Biomol. Spectrosc.* 101 (2013) 184–190.
- [33] P.P. Gan, S.H. Ng, Y. Huang, S.F. Li, Green synthesis of gold nanoparticles using palm oil mill effluent (POME): a low-cost and eco-friendly viable approach, *Bioresour. Technol.* 113 (2012) 132–135.
- [34] G. Magudapatty, P. Gangopaghyayrans, B.K. Panigrahi, K.G.M. Nair, S. Dhara, Electrical transport studies of Ag nanoparticles embedded in glass matrix, *Phys. B Condens. Matter* 299 (2001) 142–146.
- [35] S.A. Hapse, P.T. Kadaskar, A.S. Shirsath, Difference spectrophotometric estimation and validation of ibuprofen from bulk and tablet dosage form, *Der Pharm. Lett.* 3(6) (2011) 18–23.
- [36] A. Clearfield, J. Reibenspies, N. Bhuvanesh, *Principles and applications of powder diffraction*, Wiley, 2008.
- [37] M.V. Nikolić, M.Ž. Mijajlović, V.V. Jevtić, Z.R. Ratković, I.D. Radojević, Lj.R. Čomić, S.B. Novaković, G.A. Bogdanović, S.R. Trifunović, G.P. Radić, Synthesis, characterization and antimicrobial activity of copper(II) complexes with some S-alkyl derivatives of thiosalicylic acid. Crystal structure of the binuclear copper(II) complex with S-methyl derivative of thiosalicylic acid, *Polyhedron* 79 (2014) 80–87.
- [38] J.M. Andrews, BSAC standardized disc susceptibility testing method, *J. Antimicrob. Chemother.* 56 (2005) 60–76.
- [39] V. Dhand, L. Soumya, S. Bharadwaj, S. Chakra, B. Deepika, B. Sreedhar, Green synthesis of silver nanoparticles using *Coffea arabica* seed extract and its antibacterial activity, *Mater. Sci. Eng. C* 58 (2016) 36–43.
- [40] A.B.A. Boxall, Q. Chaudhry, C. Sinclair, A. Jones, R. Aitken, B. Jefferson, C. Watts, *Current and future predicted environmental exposure to engineered nanoparticles*, Central Science Laboratory Publications, York, UK, 2007, p. 89.
- [41] S.J. Klaine, P.J.J. Alvarez, G.E. Batley, T.F. Fernandes, R.D. Handy, D.Y. Lyon, S.Y. Mahendra, M.J. Mclaughlin, J.R. Lead, *Nanomaterials in the environment: behavior, fate, bioavailability, and effects*, *Environ. Toxicol. Chem.* 27(9) (2008) 1825–1851.
- [42] I. Moreno-Garrido, S. Perez, J. Blasco, Toxicity of silver and gold nanoparticles on marine microalgae, *Mar. Environ. Res.* 111 (2015) 60–73.
- [43] Ž. Mitić, M. Cakić, G.S. Nikolić, FTIR spectroscopic investigations of Co(II)–dextran complexes by using D<sub>2</sub>O isotopic exchange. In: XIII European Conference on the Spectroscopy of Biological Molecules, Palermo, Italy, 2009, p. 83.

- [44] Lj. Ilić, S. Ristić, M. Cakić, G.S. Nikolić, S. Stanković, Polynuclear complex Fe(III) with pullulan oligomers, process of its obtaining, and pharmaceutical preparations on the basis of the complex, WO Patent 2002046241A2, 2002.
- [45] G.S. Nikolić, M.D. Cakić, Physical investigation of the colloidal iron–inulin complex, *Colloid J.* 69(4) (2007), 464–473.
- [46] E. London, The molecular formula and proposed structure of the iron–dextran complex, *imferon*, *J. Pharm. Sci.* 93(7) (2004) 1838–1846.
- [47] W.F. Leech, D.G. McLaren, K.D. McSporran, Administration of copper to an animal, US Patent 2009/0029942 A1, 2009.
- [48] Ž. Mitić, G.S. Nikolić, M. Cakić, R. Nikolić, Lj. Ilić, Synthesis and spectroscopic characterization of copper(II) dextran complexes, *Russ. J. Phys. Chem.* 81(9) (2007), 1433–1437.
- [49] G.S. Nikolić, M.D. Cakić, Analysis of bioactive oligosaccharide-metal complexes by modern FTIR spectroscopy: Copper complexes, Chapter 2, pp. 15–44, In book: “Fourier transforms—New analytical approaches and FTIR strategies”, Ed. Goran Nikolic, ISBN: 978-953-307-232-6, Publisher: InTech, April 2011. Available from: <http://www.intechopen.com>
- [50] R. Bandwar, M. Sastry, R. Kadam and C. Rao, Transition-metal saccharide chemistry: synthesis and characterization of D-glucose, D-fructose, D-galactose, D-xylose, D-ribose, and maltose complexes of Co(II), *Carbohydr. Res.* 297 (1997) 333–339.
- [51] Expert Group on Vitamins and Minerals, Review of cobalt, EVM/99/19, Secretariat, UK Government, London, May 2002.
- [52] M. Cakić, Ž. Mitić, G.S. Nikolić, Lj. Ilić, G.M. Nikolić, The investigations of bioactive copper(II) complexes with reduced low-molar dextran, *Spectroscopy* 22(2, 3) (2008) 177–185.
- [53] G.S. Nikolić, M. Cakić, Ž. Mitić, Lj. Ilić, P. Premović, Attenuated total reflectance-Fourier transform infrared microspectroscopy of Cu(II) complexes with reduced dextran derivatives, *Russ. J. Phys. Chem.* 83(9) (2009) 1520–1525.
- [54] Ž. Mitić, M. Cakić, G. Nikolić, Fourier-Transform IR spectroscopic investigations of Cobalt(II)-dextran complexes by using D<sub>2</sub>O isotopic exchange, *Spectroscopy Int. J.* 24(3, 4) (2010) 269–275.
- [55] Ž.J. Mitić, G.S. Nikolić, M.D. Cakić, R.S. Nikolić, Lj.A. Ilić, The investigation of Co(II)–dextran complexes, *Chem. Ind. (Serbia)* 61(5) (2007) 257–262.
- [56] Ž. Mitić, M. Cakić, Pharmaceutically important complex compounds of some microbial exopolysaccharides, *Acta Medica Medianae* 53(4) (2014) 54–63.
- [57] M. Cakić, G. Nikolić, Lj. Ilić, FTIR spectra of iron(III) complexes with dextran, pullulan and inulin oligomers, *Bull. Chem. Technol. Macedonia* 21(2) (2002) 135–146.
- [58] M. Cakić, D. Cvetković, K. Stojanovski, P. Premović and M. Ristova, Spectroscopic study of polynuclear complex of iron(III) with hydrogenated dextran, *Spectrosc. Lett.* 9(7) (1994) 1437–1448.

- [59] V.P. Kiselev, V.P. Komar, I.V. Skornyakov, S.P. Firsov, A.D. Virnik, R.G. Zhbankov, *Spektroskopicheskoe issledovanie razlichnih strukturnih modifikacij dekstrana*, *Vysokomolek. Soedin. Serie A* 19(8) (1977) 1867–1872.
- [60] V. Seidl, O. Knop, M. Falk, *Infrared studies of water in crystalline hydrates*, *Canad. J. Chem.* 47 (1969) 1361–1368.
- [61] B. Berglund, J. Lindgren, J. Tegenfeldt, *On the correlation between deuteron quadrupole coupling constants, O-H and O-D stretching frequencies and hydrogen bond distances in solid hydrates*, *J. Mol. Struct.* 43 (1978) 179–191.
- [62] M. Kačurakova, R.H. Wilson, *Developments in mid-infrared FT-IR spectroscopy of selected carbohydrates*, *Carbohydr. Polym.* 44 (2001) 291–303.
- [63] S.Y. Lin, M.J. Li, W.T. Cheng, *FT-IR and Raman vibrational microspectroscopies used for spectral biodiagnosis of human tissues*, *Spectroscopy* 21 (2007) 1–30.
- [64] Z. Mousia, I.A. Farhat, M. Pearson, M.A. Chesters, J.R. Mitchell, *FTIR microspectroscopy study of composition fluctuations in extruded amylopectin–gelatin blends*, *Biopolymers (Biospectroscopy)* 62(4) (2001) 208–218.
- [65] W. Yu, L. Xiong, *Effect of various morphology and testing conditions on fiber infrared spectrum*, *J. Appl. Polym. Sci.* 96(4) (2005) 1003–1010.
- [66] N. Gierlinger, M. Schwanninger, *The potential of Raman microscopy and Raman imaging in plant research*, *Spectroscopy* 21(2) (2007) 69–89.
- [67] D. Chenery, H. Bowering, *Infrared and Raman spectroscopic imaging in bioscience*, *Spectrosc. Europe* 15(4) (2003) 8–14.